

Manipulation of Orbital-Angular-Momentum Spectrum Using Pinhole Plates

Yuanjie Yang^{1,2,*}, Qi Zhao,¹ Linli Liu,¹ Yidong Liu,¹ Carmelo Rosales-Guzmán,³ and Cheng-wei Qiu²

¹*School of Physics, University of Electronic Science and Technology of China, Chengdu 610054, China*

²*Department of Electrical and Computer Engineering, National University of Singapore, 117576 Singapore*

³*Wang Da-Heng Collaborative Innovation Center, Harbin University of Science and Technology, Harbin 150080, China*



(Received 7 June 2019; revised manuscript received 20 July 2019; published 4 December 2019)

The orbital angular momentum (OAM) of light has attracted a great amount of interest in recent times, due to the wide variety of applications it has made possible. Generally, the OAM spectrum is produced by coaxial superposition of several vortex beams, which might increase the complexity of the system. Here, we propose and experimentally demonstrate a simple way to produce a state of light with a controllable OAM spectrum using a binary array of pinholes. More specifically, we show that a spiral structure can convert a plane wave into a beam with a wide OAM spectrum, which can be easily tuned to pure or multiple OAM modes by adapting the structure of the pinhole plate. Furthermore, we show that a simple pinhole plate can produce structured beams with particular OAM states, such as photonic gears (superposition of OAM modes with opposite topological charges $\pm\ell$) and OAM combs (an optical mode formed by a series of discrete and equally spaced OAM modes, akin to an optical frequency comb). It is worth noting that we demonstrate the OAM comb experimentally. This study provides an avenue for the flexible generation of OAM spectra and the simplicity of the setup could make this approach convenient for many applications, such as optical communications and quantum information.

DOI: 10.1103/PhysRevApplied.12.064007

I. INTRODUCTION

Vortices are inherent to any wave phenomena and denote singular (zero intensity) points in the plane perpendicular to the propagation axis where the phase becomes indeterminate; these occur in multiples of 2π [1,2]. In general, phase singularities can be expressed mathematically as an exponential function of the form $\exp(i\ell\theta)$, where θ is the azimuthal index of the cylindrical coordinates and ℓ , known as the topological charge, is associated with an orbital angular momentum (OAM) of $\ell\hbar$ per photon, with \hbar denoting the reduced Plank constant [3,4]. The on-demand generation of optical fields embedded with OAM [5,6] has triggered a wide variety of applications [7,8], spanning fields as diverse as optical manipulation [9], classical and quantum communications [10–14], optical metrology [15–18], and imaging [19], to mention but a few. Besides optical vortices, recent studies have shown that electron [20], neutron [21], atom [22], plasmonic [23], and radio [24–27] vortices can carry OAM, leading to a wide range of applications in fields such as the manipulation of nanoparticles, memory devices, or imaging [28,29].

Over the past 20 years, a wide variety of techniques to produce vortex beam have been elucidated. Besides classic methods, based on spiral phase plates [30] or computer-generated holograms [31], the recent introduction alternative methods, namely, photon sieves [32,33] and Vogel spiral arrays [34,35], have paved the way towards the generation of OAM-carrying matter waves with electrons, atoms, or neutrons. However, most of these aforementioned methods are only able to produce modes with a unique OAM value or simple superpositions of the same. Crucially, OAM-based applications will greatly benefit from beams carrying a high-dimensional OAM spectrum [27,28], especially if this spectrum can be tailored. Recently, the applications of tailored OAM spectra have drawn much attention, for instance, to measure object parameters [36] or to perform geometric operations on images, such as rotations and reflections [37]. More recently, a quadratic phase plate has been proposed theoretically and may expand the initial single OAM mode into a comblike OAM spectrum [38].

Here, we propose a technique based on the use of a structured pinhole plate for generating structured beams with a particular OAM spectrum. We first simulate these structures and then experimentally corroborate the quality of the generated beams. More specifically, we measure the

*dr.yang2003@uestc.edu.cn

OAM spectrum using a modal decomposition technique [39], which confirms that the experimental results agree well with our simulations. We demonstrate our technique with two examples, namely, a photonic gear and an OAM comb. Further, it is worth noting that our technique not only applies to light waves, but it can also apply to matter waves, such as electron and neutron beams.

II. THOERY

A. Generation of OAM spectra: From a wide spectrum to a single mode

To explain our method, let us analyze the case of a plane wave $u(x, y, z)$ passing through a ring slit represented by an aperture function $T(x_0, y_0)$, as shown in Fig. 1(a). Fresnel diffraction theory provides a powerful method to find the complex optical field at a given observation plane along the propagation direction, for example, the z axis [40],

$$u(x, y, z) = \frac{e^{ikz}}{i\lambda z} \int \int_{-\infty}^{\infty} T(x_0, y_0) e^{\frac{ik}{2z}[(x-x_0)^2 + (y-y_0)^2]} dx_0 dy_0, \quad (1)$$

where λ is the wavelength and k is the wave number. The intensity pattern of the field diffracted by the ring slit

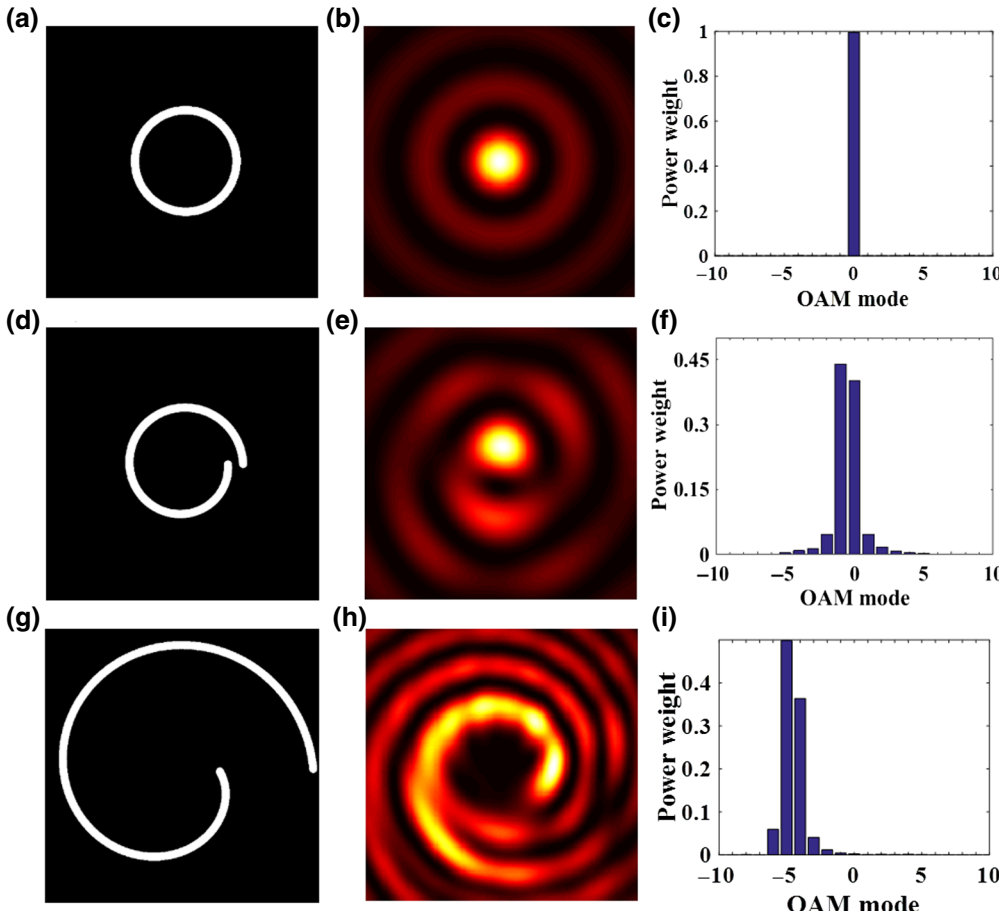


[Fig. 1(a)] is shown in Fig. 1(b). To measure its OAM spectrum, remember that any light beam can be expressed as a weighted superposition of Laguerre-Gaussian (LG) modes as [41,42]

$$u(x, y, z) \propto \sum_{p=0}^{\infty} \sum_{\ell=-\infty}^{\infty} c_{p,\ell} \varphi_{p,\ell}(x, y, z), \quad (2)$$

where $\varphi_{p,\ell}(x, y, z)$ represents the set of LG modes. Moreover, $c_{p,\ell}$ are weighting coefficients that can be computed as

$$c_{p,\ell} = \iint u(x, y, z) \varphi_{p,\ell}^*(x, y, z) dx dy, \quad (3)$$

where $*$ denotes the complex conjugate.

This method enables the OAM spectrum of any field $u(x, y, z)$ to be computed. In particular, the OAM spectrum of a ring slit is illustrated in Fig. 1(c) and features a unique peak at $\ell = 0$. Clearly, a ring slit adds no OAM to a diffracted plane wave. In fact, it is not difficult to understand this, since we know that when a plane wave passes through a ring slit it generates a zero-order Bessel beam of topological charge $\ell = 0$. However, if we change the ring aperture to a spiral aperture [see Figs. 1(d) and 1(g)],

FIG. 1. Schematics of the binary slits. (a) Ring slit and (d) and (g) spiral slits of different radii; (b),(e),(h) the corresponding simulated intensity profiles, and (c),(f),(i) the OAM spectra of the diffracted beam at $z = 1$ m, when the plates are illuminated with a plane wave of wavelength $\lambda = 532.8$ nm.

the diffracted beam, the intensity of which is shown in Figs. 1(e) and 1(h), respectively, acquires a wider OAM spectrum [see Figs. 1(f) and 1(i)]. Importantly, the OAM spectrum can be tuned by tuning the shape of the spiral slit [see Figs. 1(g)–1(i)]. That is, the shape of the spiral slit induces a redistribution of the azimuthal phase, giving rise to a beam with a spiral phase profile and a wider OAM spectrum centered at a particular ℓ value. More specifically, the spiral shown in Fig. 1(d) produces an OAM spectrum centered at $\ell = -1$, while the spiral shown in Fig. 1(g) features an OAM spectrum centered at $\ell = -5$. The relationship between the shape of the slit and the central topological ℓ is governed by $r_\alpha = (\ell z \lambda \alpha / \pi + r_0^2)^{1/2}$, where r_α indicates the radius of the slit at angle α , r_0 is the minimum radius of the slit, and z is the distance of the observation plane [40]. As shown below, similar results are obtained with a discretized version of the spiral slit; this is an array of pinholes that follow the same trend. However, this type of pinhole mask enables the generation of more complicated structures, giving rise to a wide variety of structured beams of light or matter [36].

The discretized version of the spiral slit consists of a number of pinholes located at a specific position [see Fig. 2(a)], the azimuthal angle and radius of the n th pinhole, measured from the center, are given by $\alpha_n = 2\pi n/N$

and $r_n = (\ell z \lambda \alpha_n / \pi + r_0^2)^{1/2}$, respectively. Here, N is the number of pinholes, λ is the wavelength, r_0 is the distance from the center to the first pinhole, and z is the distance from the slit to the observation plane [40,43]. By comparing Figs. 1(g)–1(i) and 2(a)–2(c), it is easy to see that not only the intensity [Figs. 1(h) and 2(b)], but also the OAM spectra [Figs. 1(i) and 2(c)] for both the continuous and discretized spiral slits are almost identical. Hence, this simple technique enables a continuous or discrete spiral slit to reshape, as desired, the OAM spectrum of a plane wave, thus allowing full control of the OAM spectrum.

Tuning of the OAM spectrum to a specific value can be achieved by adding several copies of identical spirals equally distributed along the azimuthal direction, as illustrated in Figs. 2(d) and 2(g). For example, there are five and six spirals in Figs. 1(d) and 1(g), respectively; accordingly, beams with specific OAM values of $\ell = -5$ and -6 are generated, respectively, as shown in Figs. 2(f) and 2(i). This technique can be explained by the OAM selection principle of rotationally symmetric structures [36], which states that an m -order rotationally symmetric structure can select the OAM modes that are multiples of m , depleting the rest. This is why the OAM spectra shown in Figs. 2(f) and 2(i) clearly show unique OAM values at $\ell = -5$ and -6 , respectively.

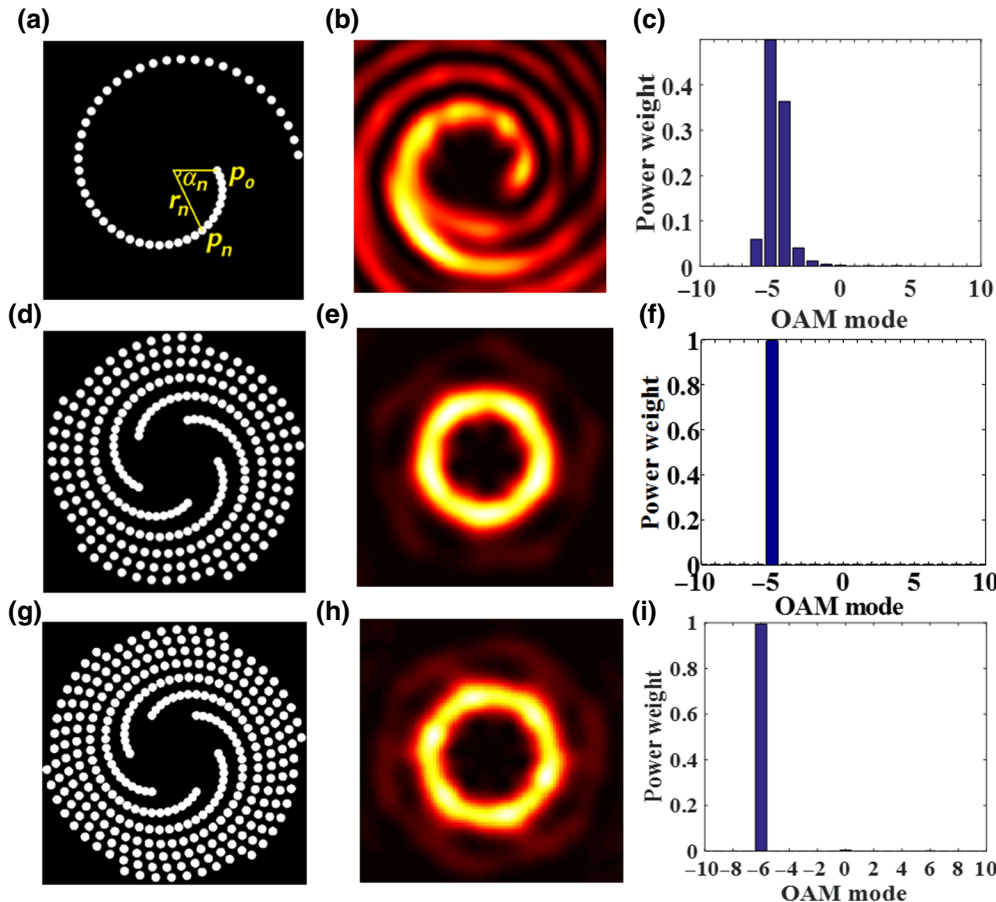


FIG. 2. Schematics of the discretized binary slits. (a) Single spiral, (d) five spirals, and (g) six spirals; (b),(e),(h) the corresponding simulated intensity profiles; and (c),(f),(i) the OAM spectra of the diffracted beam at $z = 1$ m, when the plates are illuminated with a plane wave of wavelength $\lambda = 532.8$ nm.

B. Generation of petal-like structures with opposite OAM modes

Recently, the superposition of two vortex beams with topological charge $\pm\ell$, namely, photonic gears, have attracted significant attention [44–46]. D’Ambrosio *et al.* demonstrated that photonic gears greatly enhanced the angular measurement precision [44]. Lavery *et al.* demonstrated that photonics gears could be used to detect the angular speed of a spinning object [45]. Now, we show how to produce photonic gears using our method. To generate such a pair of OAM modes, we need to combine two spiral masks with opposite ℓ values. The azimuthal and radial distributions of the n th pinhole in the m th spiral are

$$\alpha_{m,n} = \pm \left(\frac{2\pi n}{N} + \frac{2\pi m}{M} \right) \quad (4)$$

and

$$r_n = \pm \left(\frac{\ell z \lambda \alpha_n}{\pi} + r_0^2 \right)^{1/2}, \quad (5)$$

respectively. Figures 3(a), 3(d), and 3(g) show the binary mask that generates the superposition of modes $\ell = \pm 2$, $\ell = \pm 4$, and $\ell = \pm 5$, respectively. It is known the superposition of two vortex beams of opposite topological

charges ($\pm\ell$) generate an intensity pattern consisting of 2ℓ petal-like structures [47,48]. This is clearly shown in the simulated intensity pattern of the diffracted wave [see Figs. 3(b), 3(e) and 3(h)]. Traditionally, petal-like beams are generated, for example, by a coaxial superposition of two vortex beams; here, we show that a simpler method consisting of a plate with properly arranged pinholes can produce the same effect. The corresponding OAM mode spectra shown in Figs. 3(c), 3(f), and 3(i) demonstrate that the generated OAM modes are highly pure.

C. Generation of OAM comb

It is well known that an optical frequency comb, which is a laser spectrum consisting of a series of discrete and equally spaced frequency lines, are widely used in optical metrology, optical atomic clocks, precise GPS technology, etc. [49,50]. Now, we want to show that we can produce an OAM comb in a very simple way, which consists of a series of discrete equally spaced OAM modes. Figure 4(a) shows a simple diffraction screen with two pinholes, and Fig. 4(b) shows the intensity pattern when a plane wave illuminates such a screen; this is the famous Young’s interference experiment. Interestingly, as shown in Fig. 4(c), the OAM spectrum of the diffracted field features a series of discrete equally spaced OAM modes, which we refer

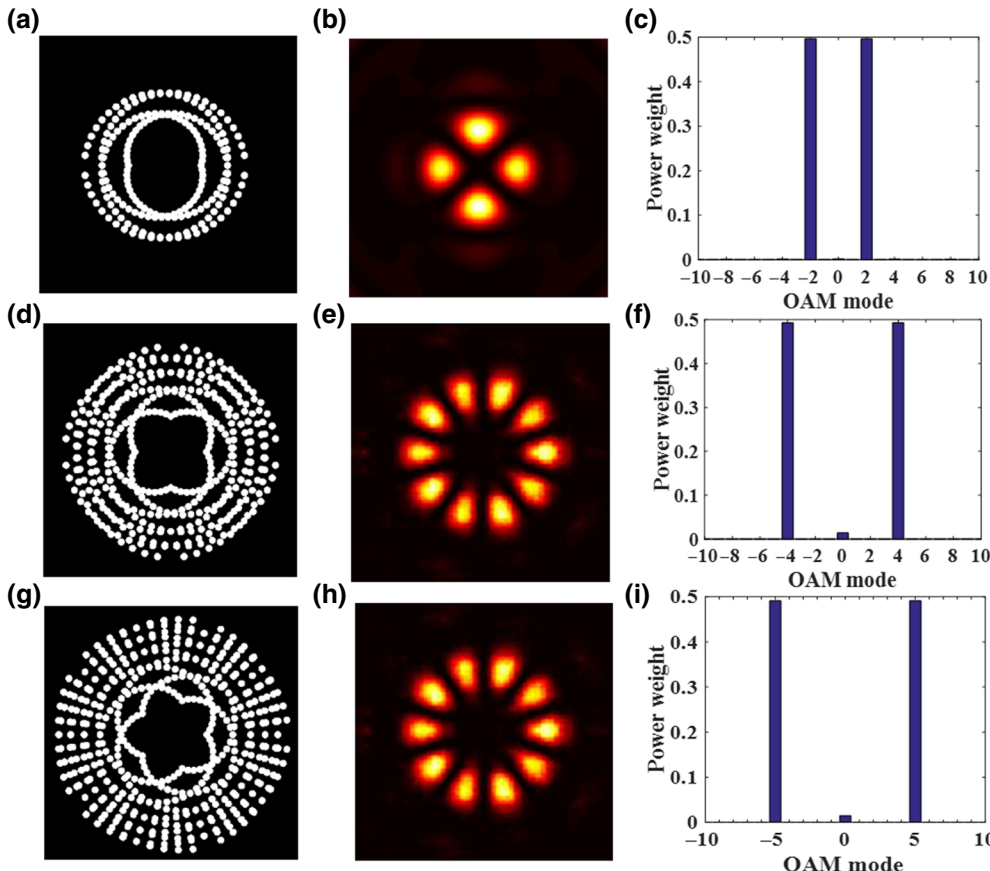


FIG. 3. Schematics of the generation of petal-like beams with opposite OAM modes. (a) Simulated mask for $\ell = \pm 2$; (b),(c) the corresponding simulated intensity profiles and OAM spectrum; (d)–(f) same as (a)–(c), but $\ell = \pm 4$; and (g)–(i) same as (a)–(c), but $\ell = \pm 5$.

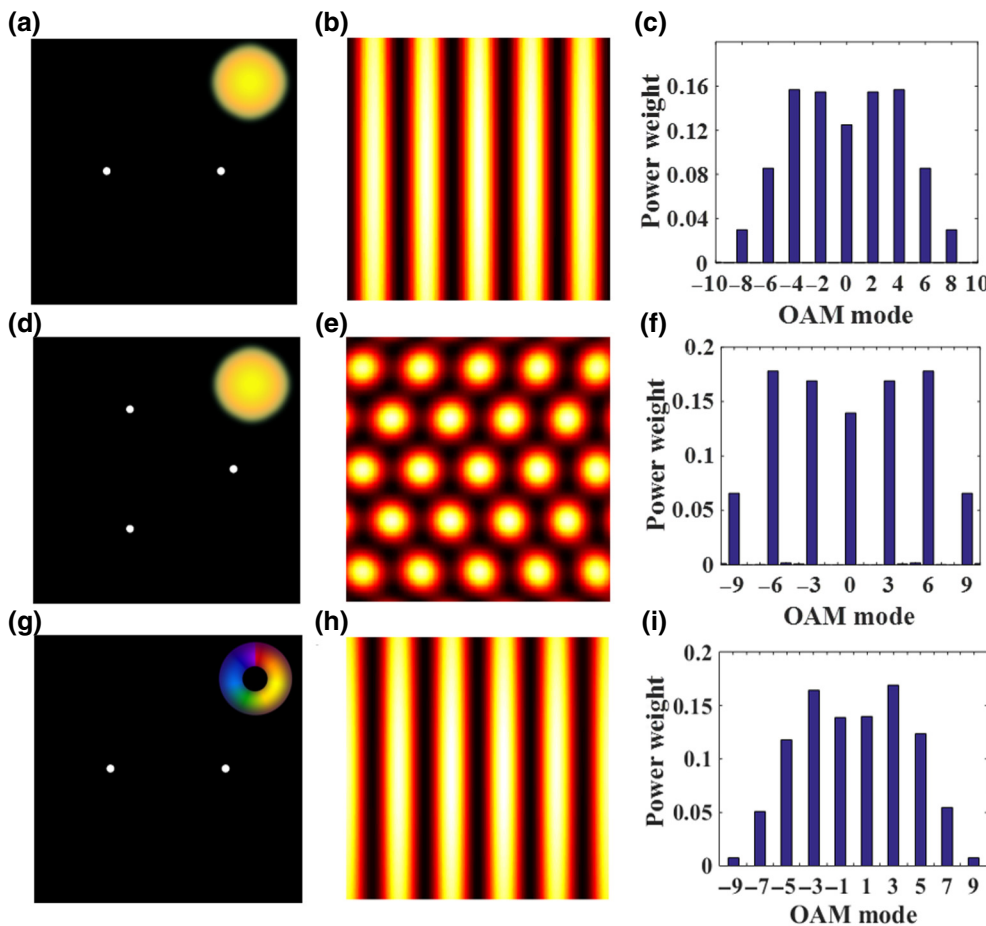


FIG. 4. Schematics of the generation of OAM comb. Two and three pinhole plate (left column). The insets in (a),(d) represent a plane wave, whereas those in (g) represent an optical vortex of topological charge $\ell = 1$. Corresponding simulated intensity profile (middle row). OAM spectrum of the generated output field (right column).

to as the OAM comb. Crucially, this OAM spectrum only contains OAM modes that are in the form $\ell = \pm 2, \pm 4, \pm 6, \dots$ Figures 4(d)–4(f) show a similar phenomenon for a three-pinhole plate. Again, the OAM spectrum contains only OAM modes of the form $\ell = \pm 3, \pm 6, \pm 9, \dots$ That is, a plane wave diffracted by a simple pinhole plate

generates an OAM comb consisting of modes that multiply the number of pinholes. If, instead of a plane wave, we use a vortex beam to illuminate the two-pinhole plate, the OAM comb will shift in proportion to the OAM value on the incident field. Figure 4(i) shows the OAM spectrum for the specific case $\ell = 1$, where we can see that

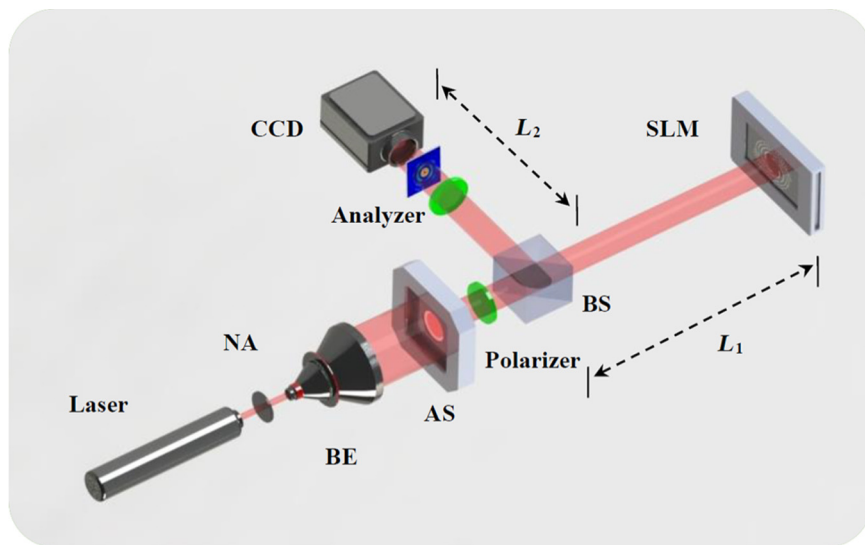


FIG. 5. Schematic of the experimental setup. NA denotes neutral attenuators, BE denotes the beam expander, AS denotes the aperture slot, BS denotes the beam splitter, and CCD denotes the charge-coupled device. The sum of distances L_1 and L_2 is equal to the distance of z in Eq. (5).

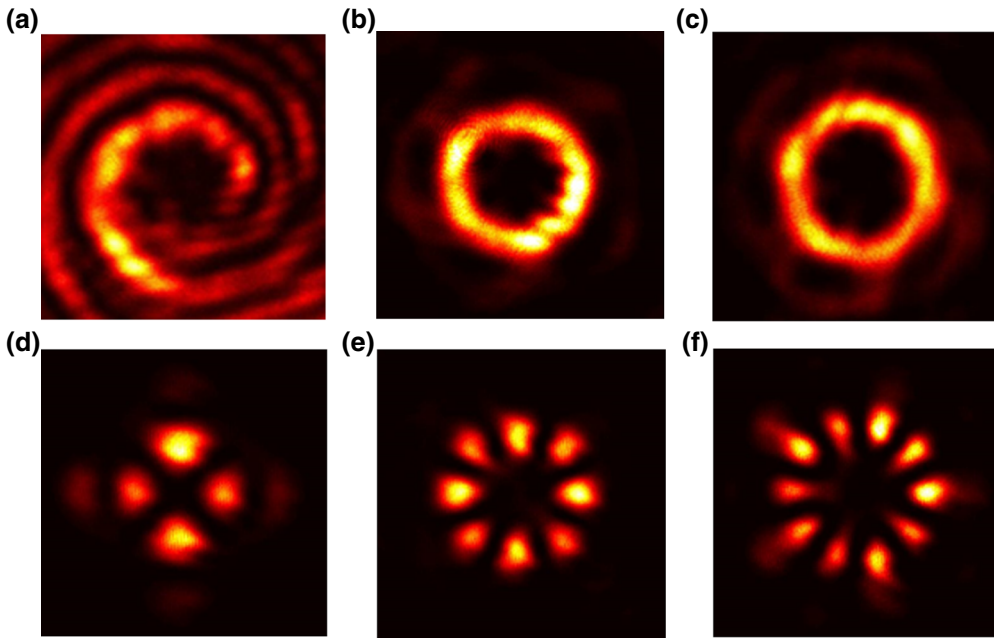


FIG. 6. Experimental results of generated structured beams with OAM modes. (a)–(c) The corresponding experimental results to those in Figs. 2(b), 2(e) and 2(h). (d)–(f) The corresponding experimental results to those in Figs. 3(b), 3(e) and 3(h).

the OAM modes have shifted to $\ell_0 = 1$. Therefore, the OAM modes in an OAM comb are given by $\ell_n = n\ell_r + \ell_0$, where n is a integer, ℓ_r is the comb repetition rate, and ℓ_0 is the offset of the comb, which is dependent on the incident beam.

III. EXPERIMENTAL RESULTS AND DISCUSSION

To validate our simulations described above, an experimental proof-of-concept corroboration was carried out and presented next. In our experiments we used a multihole plate, which we generated with a spatial light

modulator (SLM), but it can also be generated with a digital micromirror device (DMD) or a physical plate with pinholes. A sketch of the experimental setup is depicted in Fig. 5. A He-Ne laser beam properly expanded and collimated by a BE, illuminates a reflective SLM (Holoeye, LC-R 1080), where the binary structured sieve is displayed. A beam splitter placed before the SLM redirects the shaped beam, coming from the SLM, towards a CCD camera (pixel size $3.45 \times 3.45 \mu\text{m}^2$, 1920 × 1080 pixels), where the generated beam is recorded. Since the SLM only modulates horizontally polarized light, a polarizer is inserted before the SLM to match its polarization.

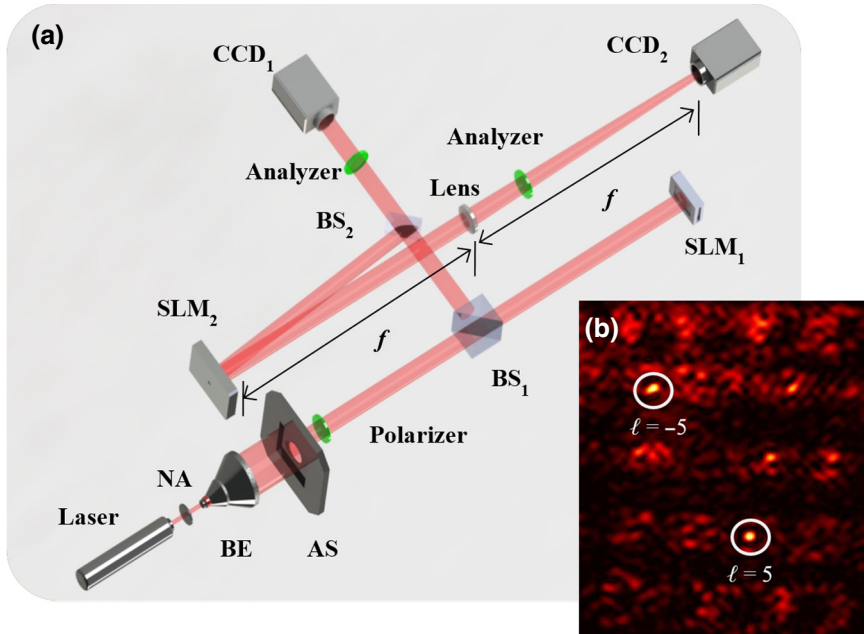


FIG. 7. (a) Experimental setup used to measure OAM spectra of photonic gears. f is the focal length of the lens, BS_1 and BS_2 are beam splitters, SLM_2 denotes the phase-only spatial light modulator, CCD_2 is the image sensor used to detect the mode decomposition by SLM_2 . (b) Far-field intensity of multiplexed set of modes projected by topological input modes of $\ell = \pm 5$.

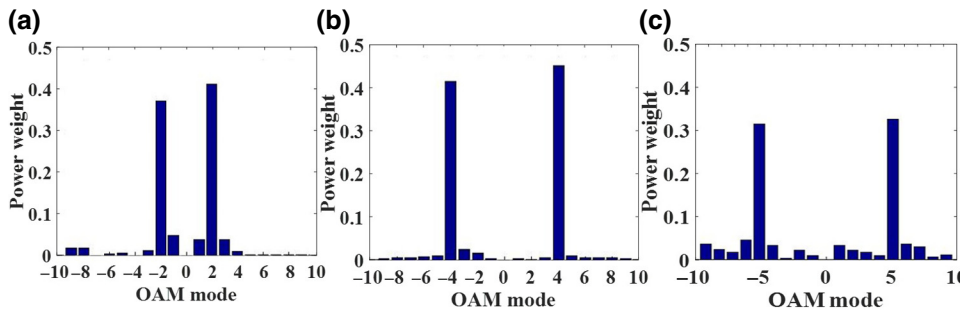


FIG. 8. Experimentally measured OAM spectra. (a)–(c) The corresponding experimental results to those in Figs. 3(c), 3(f), and 3(i), respectively.

Additionally, a second polarizer is placed before the CCD to filter out a coherent optical background [51].

The experimental results of the intensity profiles measured on the CCD are shown in Fig. 6, which correspond to the simulations shown in Figs. 2 and 3. From the comparison, we can see that the experimental results are in high concordance with the simulations, which demonstrate that the structured pinhole plates are practical for generating photonic gears.

To measure experimentally the OAM spectra of the generated beams, we perform a modal decomposition [39,52]. Without the loss of generality, we measure only the OAM spectrum of photonic gears, namely, the superposition of two OAM modes with topological charge $\pm\ell$. It is known that the composite OAM spectrum of the generated beams can be determined by measuring the far-field intensity when we project the input beams into a set of orthogonal OAM modes [39]. Even though, in principle, we have to project the input field into an infinite set of OAM modes, in practice we only require a small subset, which, in our experiments, is $\ell \in [-9, 10]$. Figure 7(a) shows a schematic representation of the implemented experimental setup that allows us to measure the OAM spectrum. The generated photonic gears after SLM₁ are projected onto phase-only SLM₂ (Holoeye, PLUTO VIS) using a second beam splitter (BS₂). The light modulated by SLM₂ is Fourier transformed using a lens with a focal length of $f/3 = 500$ mm and imaged onto CCD₂. As an example, the far-field intensity pattern of the generated beam ($\ell = \pm 5$), projected onto the multiplexed subset of modes encoded on SLM₂, is shown in Fig. 7(b). The on-axis intensity spots at $\ell = \pm 5$, shown in Fig 7(b), indicate their topological charges.

The experimental results of the OAM spectrum measured on CCD₂ are shown in Fig. 8, which correspond to the simulations in Figs. 3(c), 3(f), and 3(i). From the comparison, we can see that the experimental results are in high concordance with the simulations; this demonstrates that the structured photon sieves are practical for the generation of photonic gears.

IV. CONCLUSIONS

Here, we provide a technique to manipulate the OAM spectrum based on the use of pinhole plates, and the

concept OAM comb is proposed. Our study provides an alternative view for understanding OAM and the generation of the superposition of OAM modes. The ability to generate a light beam with a specifically tailored spectrum is crucial for OAM applications, and our study may find potential applications in many OAM-based systems. In particular, the OAM comb, which is a kind of tailored OAM spectrum, may find applications in many fields, such as a field analyzer for determining the dimensionality of multimode fields [53]. Although the concept is tested with optical vortex beams, this is not confined to the optical regime and can be used for the generation of any other composite scalar vortices, such as electron, neutron, acoustic, and radio vortices.

ACKNOWLEDGMENTS

This work is supported by the National Natural Science Foundation of China (Grants No. 11874102 and No. 11474048), and the National Research Foundation, Prime Minister's Office, Singapore, under its Competitive Research Program (CRP) (NRF-CRP15-2015-03). We acknowledge Dr. Ruifang Liu for valuable discussions.

- [1] J. F. Nye and M. V. Berry, Dislocations in wave trains, *Proc. R. Soc. London, A* **336**, 165 (1974).
- [2] L. Allen, M. J. Padgett, and M. Babiker, The orbital angular momentum of light, *Prog. Opt.* **39**, 291 (1999).
- [3] L. Allen, M. W. Beijersbergen, R. J. C. Spreeuw, and J. P. Woerdman, Orbital Angular-Momentum of Light and the Transformation of Laguerre–Gaussian Laser Modes, *Phys. Rev. A* **45**, 8185 (1992).
- [4] S. J. van Enk and G. Nienhuis, Angular momentum in evanescent waves, *Opt. Commun.* **94**, 147 (1992).
- [5] A. Forbes, A. Dudley, and M. McLaren, Creation and detection of optical modes with spatial light modulators, *Adv. Opt. Photonics* **8**, 200 (2016).
- [6] N. Savage, Spectrometers, *Nat. Photonics* **3**, 170 (2009).
- [7] H. Rubinsztein-Dunlop *et al.*, Roadmap on structured light, *J. Opt.* **19**, 013001 (2017).
- [8] M. Yao and J. Padgett, Orbital angular momentum: Origins, behavior and applications, *Adv. Opt. Photonics* **3**, 161 (2011).

- [9] K. Dholakia and T. Cizmar, Shaping the future of manipulation, *Nat. Photonics* **5**, 335 (2011).
- [10] J. Wang, J. Yang, I. Fazal, N. Ahmed, Y. Yan, H. Huang, Y. Ren, Y. Yue, S. Dolinar, M. Tur, and A. E. Willner, Terabit free-space data transmission employing orbit angular momentum multiplexing, *Nat. Photonics* **6**, 488 (2012).
- [11] N. Bozinovic, Yang Yue, Y. Ren, M. Tur, P. Kristensen, Hao Huang, A. E. Willner, and S. Ramachandran, Terabit-scale orbital angular momentum mode division multiplexing in fibers, *Science* **340**, 1545 (2013).
- [12] G. Gibson, Johannes Courtial, M. Padgett, M. Vasnetsov, V. Pas'ko, S. Barnett, and S. Franke-Arnold, Free-space information transfer using light beams carrying orbital momentum, *Opt. Express* **22**, 5448 (2004).
- [13] T. Lei, M. Zhang, Y. Li, P. Jia, G. Liu, X. Xu, Z. Li, C. Min, J. Lin, C. Yu, H. Niu, and X. Yuan, Massive individual orbital angular momentum channels for multiplexing enabled by dammann gratings, *Light Sci. Appl.* **4**, e257 (2015).
- [14] A. Trichilli, C. Rosales-Guzmán, A. Dudley, B. Ndagano, A. Salem, M. Zghal, and A. Forbes, Optical communication beyond orbital angular momentum, *Sci. Rep.* **6**, 27674 (2016).
- [15] A. Belmonte and J. P. Torres, Optical Doppler shift with structured light, *Opt. Lett.* **36**, 4437 (2011).
- [16] C. Rosales-Guzmán, N. Hermosa, A. Belmonte, and J. P. Torres, Experimental detection of transverse particle movement with structured light, *Sci. Rep.* **3**, 2815 (2013).
- [17] C. Rosales-Guzmán, N. Hermosa, A. Belmonte, and J. P. Torres, Measuring the translational and rotational velocities of particles in helical motion using structured light, *Opt. Express* **22**, 16504 (2014).
- [18] A. Belmonte, C. Rosales-Guzmán, and J. P. Torres, Measurement of flow vorticity with helical beams of light, *Optica* **2**, 1002 (2015).
- [19] L. Chen, J. Lei, and J. Romero, Quantum digital spiral imaging, *Light Sci. Appl.* **3**, e153 (2014).
- [20] J. Verbeeck, H. Tian, and P. Schattschneider, Production and application of electron vortex beams, *Nature* **467**, 301 (2010).
- [21] C. W. Clark, R. Barankov, M. G. Huber, M. Arif, D. G. Cory, and D. A. Pushin, Controlling neutron orbital angular momentum, *Nature* **525**, 504 (2015).
- [22] V. E. Lembessis, D. Ellinas, M. Babiker, and O. Al-Dossary, Atom Vortex Beams, *Phys. Rev. A* **89**, 053616 (2014).
- [23] H. Kim, J. Park, S. Cho, S. Lee, M. Kang, and B. Lee, Synthesis and dynamic switching of surface plasmon vortices with plasmonic vortex lens, *Nano Lett.* **10**, 529 (2010).
- [24] B. Thidé, H. Then, J. Sjoholm, K. Palmer, J. E. S. Bergman, T. D. Carozzi, Y. N. Istomin, N. H. Ibragimov, and R. Khamitova, Utilization of Photon Orbital Angular Momentum in the Low-Frequency Radio Domain, *Phys. Rev. Lett.* **99**, 087701 (2007).
- [25] M. Barbuto, F. Bilotti, and A. Toscano, Patch antenna generating structured fields with a Möbius polarization state, *IEEE Antennas Wirel. Propag. Lett.* **16**, 1345 (2017).
- [26] F. Tamburini, E. Mari, A. Sponselli, B. Thidé, A. Bianchini, and F. Romanato, Encoding many channels on the same frequency through radio vorticity: First experimental test, *New J. Phys.* **14**, 033001 (2012).
- [27] M. Barbuto, M.-A. Miri, A. Alù, F. Bilotti, and A. Toscano, Exploiting the topological robustness of composite vortices in radiation systems, *Prog. Electromag. Res.* **162**, 39 (2018).
- [28] R. A. Herring, A new twist for electron beams, *Science* **331**, 155 (2011).
- [29] J. Harris, V. Grillo, E. Mafakheri, G. C. Gazzadi, S. Frabboni, R. W. Boyd, and E. Karimi, Structured quantum waves, *Nat. Phys.* **11**, 629 (2015).
- [30] M. W. Beijersbergen, R. P. C. Coerwinkel, and M. Kristensen, Helical-wavefront laser beams produced with spiral phase plate, *Opt. Commun.* **112**, 321 (1994).
- [31] N. R. Heckenberg, R. McDuff, C. P. Smith, and A. G. White, Generation of optical phase singularities by computer-generated holograms, *Opt. Lett.* **17**, 221 (1992).
- [32] R. Liu, F. Li, M. J. Padgett, and D. B. Philips, Generalized photon sieves: Fine control of complex fields with simple pinhole arrays, *Optica* **2**, 1028 (2015).
- [33] K. Huang, H. Liu, F. J. Garcia-Vidal, M. Hong, B. Luk'yanchuk, J. Teng, and C. Qiu, Ultrahigh-capacity non-periodic photon sieves operating in visible light, *Nat. Commun.* **6**, 7059 (2015).
- [34] N. Lawrence, J. Trevino, and L. Dal Negro, Control of optical orbital angular momentum by Vogel spiral arrays of metallic nanoparticles, *Opt. Lett.* **37**, 5076 (2012).
- [35] Y. Yang, G. Thirunavukkarasu, M. Babiker, and J. Yuan, Orbital-Angular-Momentum Mode Selection by Rotationally Symmetric Superposition of Chiral States with Application to Electron Vortex Beams, *Phys. Rev. Lett.* **119**, 094802 (2017).
- [36] G. Xie, H. Song, Z. Zhao, G. Milione, Y. Ren, C. Liu, R. Zhang, C. Bao, L. Li, Z. Wang, K. Pang, D. Starodubov, B. Lynn, M. Tur, and A. E. Willner, Using a complex optical orbital-angular-momentum spectrum to measure object parameters, *Opt. Lett.* **42**, 4482 (2017).
- [37] F. Li, T. Xu, W. Zhang, X. Qiu, X. Lu, and L. Chen, Optical images rotation and reflection with engineered orbital angular momentum spectrum, *Appl. Phys. Lett.* **113**, 161109 (2018).
- [38] H. Liu, C. Teng, H. Yang, H. Deng, R. Xu, S. Deng, M. Chen, and L. Yuan, Proposed phase plate for superimposed orbital angular momentum state generation, *Opt. Express* **26**, 14792 (2018).
- [39] A. Vijayakumar, C. Rosales-Guzmán, M. R. Rai, J. Rosen, O. V. Minin, I. V. Minin, and A. Forbes, Generation of structured light by multilevel orbital angular momentum holograms, *Opt. Express* **27**, 6459 (2019).
- [40] Y. Yang, X. Zhu, J. Zeng, X. Lu, C. Zhao, and Y. Cai, Anomalous Bessel vortex beam: Modulating orbital angular momentum with propagation, *Nanophotonics* **7**, 677 (2018).
- [41] G. Molina-Terriza, J. P. Torres, and L. Torner, Management of the Angular Momentum of Light: Preparation of Photons in Multidimensional Vector States of Angular Momentum, *Phys. Rev. Lett.* **88**, 013601 (2001).
- [42] E. Hemsing, A. Knyazik, M. Dunning, D. Xiang, A. Marinelli, C. Hast, and J. B. Rosenzweig, Coherent optical vortices from relativistic electron beams, *Nat. Phys.* **9**, 549 (2013).
- [43] Z. Li, M. Zhang, G. Liang, X. Li, X. Chen, and C. Cheng, Generation of high-order optical vortices with

- asymmetrical pinhole plate under plane wave illumination, *Opt. Express* **21**, 15755 (2013).
- [44] V. D'Ambrosio, N. Spagnolo, L. Del Re, S. Slussarenko, Y. Li, L. C. Kwek, L. Marrucci, S. P. Walborn, L. Aolita, and F. Sciarrino, Photonic polarization gears for ultra-sensitive angular measurements, *Nat. Commun.* **4**, 2432 (2013).
- [45] M. P. J. Lavery, F. C. Speirits, S. M. Barnett, and M. J. Padgett, Detection of spinning object using light's orbital angular momentum, *Science* **341**, 537 (2013).
- [46] H. Li, M. J. Strain, L. Meriggi, L. Chen, J. Zhu, K. Cicek, J. Wang, X. Cai, M. Sorel, M. G. Thompson, and S. Yu, Pattern manipulation via on-chip phase modulation between orbital angular momentum beams, *Appl. Phys. Lett.* **107**, 051102 (2015).
- [47] W. Zhang, Q. Qi, J. Zhou, and L. Chen, Mimicking Faraday Rotation to Sort the Orbital Angular Momentum of Light, *Phys. Rev. Lett.* **112**, 153601 (2014).
- [48] M. Padgett, J. Arlt, N. Simpson, and L. Allen, An experiment to observe the intensity and phase structure of Laguerre-Gaussian laser modes, *Am. J. Phys.* **64**, 77 (1996).
- [49] P. Del'Haye, A. Schliesser, O. Arcizet, T. Wilken, R. Holzwarth, and T. J. Kippenberg, Optical frequency comb generation from a monolithic microresonator, *Nature* **450**, 1214 (2007).
- [50] A. M. Weiner, Frequency combs: Cavity solitons come of age, *Nat. Photonics* **11**, 533 (2017).
- [51] F. Ricci, W. Löffler, and M. P. van Exter, Instability of higher-order optical vortices analyzed with a multi-pinhole interferometer, *Opt. Express* **20**, 22961 (2012).
- [52] C. Schulze, A. Dudley, D. Flamm, M. Duparre, and A. Forbes, Measurement of the orbital angular momentum density of light by modal decomposition, *New J. Phys.* **15**, 073025 (2013).
- [53] J. B. Pors, A. Aiello, S. S. R. Oemrawsingh, M. P. van Exter, E. R. Eliel, and J. P. Woerdman, Angular Phase-Plate Analyzers for Measuring the Dimensionality of Multimode Fields, *Phys. Rev. A* **77**, 033845 (2008).